9th Asia-Pacific Conference on Wind Engineering
Auckland, New Zealand
3-7 December 2017

Recent advances and challenges for the non-flutter design principle

M.S. Andersen[1] and A. Brandt[2]

[1] Ph.D. Student, Department of Civil and Architectural Engineering

University of Southern Denmark, Campusvej 55, DK-5230, Odense M, Denmark

[2] Associate Professor, Department of Mechanical Engineering

University of Southern Denmark, Campusvej 55, DK-5230, Odense M, Denmark

Abstract

A novel triple box girder design have been developed and is presented in the present paper. It performs aerodynamically stable up to 88 m/s at a torsional-to-vertical frequency ratio of 1.21, which might be interesting for future long span suspension bridges spanning between 2 and 4 km. The steady aerodynamic moment coefficient is negative and shows non-linear behaviour at angles of attack close to zero. The aerodynamic derivatives are estimated by harmonic forced motion tests. A digital linear phase bandpass filter around the harmonic excitation frequency is used in order to avoid alienation from forces at other frequencies. It is found that the torsional stiffness is critical for the free response in wind. An artificial reduction of the torsional stiffness (and torsional-to-vertical frequency ratio) results in limit cycle oscillations with high amplitudes.

Introduction

The field of bridge aerodynamics has come a long way since the Tacoma Narrows disaster in 1940. The tendency of increasing span lengths of suspension bridges has continuously challenged the aerodynamic and structural design of the deck.

Today it is likely that the main span lengths will soon exceed 2000 m, e.g. in the Ferry-free coastal route E39 project in Norway. This calls for innovative solutions to reduce the wind loads and not least to ensure adequate safety against aerodynamic instabilities of the bridge deck in terms of flutter and static divergence. If no measures are taken, the critical wind speeds for flutter and torsional divergence decreases with the span length [1].

The critical wind speeds can be enhanced by added structural mass, but since the mass is critical for the cost of the bridge, the best solution is a light-weight solution.

The most radical solution put forward in the literature to avoid classical flutter was introduced by Richardson in 1981 [6] where the vertical and torsional natural frequencies, f_h and f_α were made identical. Several studies, e.g. [3-5], confirm this, either theoretically or experimentally. Richardson's [6] twin box concept is illustrated by the principal cross section shown in Figure 1.

Figure 1. Twin box design with four main cables introduced by Richardson in [6]. Cross girders connect the twin boxes and the centre of rotation is located in the centre of the gap

It is not possible to obtain a torsional frequency equal to or lower than the vertical frequency when the radius of gyration of the deck is smaller than the distance from the main cables to the axis of rotation. Therefore, later studies [2, 3, 6] have considered a similar design as shown in Figure 1, but without the outer main cables, see Figure 2.

Figure 2. Non-flutter twin box design where the decks are located external to the main cables. To the author's knowledge, this design was first proposed in [8]

In [2] it was found that multi-modal flutter is unlikely to occur due to shape wise dissimilarity between torsional modes of higher order and vertical modes of lower order. Section model tests reported in [3] showed that static divergence could be avoided at high wind speeds when the torsional and vertical frequencies were identical, but mean rotations of the deck were reported to be approximately $\alpha \approx 8°$ deg. at the highest wind speeds. In [1] it was seen that steady state oscillations tend to follow after the onset of increasing mean rotations. A peak in the RMS values of the rotation for configuration 4 at medium-high wind speeds in [3] might indicate the same.

An issue with the twin box design shown in Figure 2 is the eccentricity of traffic loads [8] which may cause unacceptable large mean rotations if only one lane is loaded with traffic. Instead of a twin box design, it might be feasible to use a triple box girder as shown in Figure 3 where the car lanes are held on the central deck and pedestrians on the decks external to the main cables.

Such a wide cross sectional design will increase the torsional aerodynamic damping and the necessary torsional stiffness might be obtained by having a large distance between the main cables. The need for torsional stiffness of the decks are therefore lower and shallower streamlined boxes could be used.

Figure 3. The present triple box girder design configured to have a lower torsional than vertical frequency. The central deck is for the heavy traffic while the decks external to the main cables are for pedestrians and bicycles only

The aerodynamics of a bridge section model similar to Figure 3 (without the main cables) has recently been studied in the wind tunnel facilities at FORCE Technology, Denmark. The static

force coefficients, aerodynamic derivatives and the aerodynamic stability limits at several different torsional-to-vertical frequency ratios, $\gamma_\omega = f_\alpha/f_h$ have been estimated. The present paper includes a selection of the most important results. The challenges for the non-flutter design principle where the torsional frequency deliberately is equal to or lower than the vertical are finally discussed at the end of the paper.

Section model

The width of the tested section model including the gaps is $B = 1.2$ m. The width of the central deck is $B_c = 0.318$ m while the depth of the central deck is $D_c = 0.04$ m at the centre line. The inclination from the centre line towards the edges is -3/100. The wind noses consist of equilateral triangles where each side is 0.036 m. The external boxes were constructed as sharp-edged $B_e/D_e = 10$ rectangular sections where $B_e = 0.07$ m. The railings are shown in Figure 4. The section models were not considered for any particular full-scale prototype bridge, but as a conceptual study of a suspension bridge with stiff backstays spanning 2100 m. The geometric scale of $\lambda = 1{:}50$ was used. The length of the section model was $L = 2.55$ m and cross girders connected the central box with the external boxes for each 0.516 m. The natural bending frequency of the section model when clamped in the test rig was estimated to $f_b = 10.5$ Hz and a torsional frequency was found at $f_t = 9.1$ Hz. The tunnel test section was 2.6 m × 1.8 m. End plates were not used. It was assumed that end effects were negligible because the section spanned across the tunnel close to the walls. Tunnel blockage is an issue with a wide section during large rotations. The large gaps were considered to reduce the blockage effects. All tests were conducted under laminar flow conditions. The turbulence intensity in the incoming wind was measured to approximately $I_u = 0.1\%$.

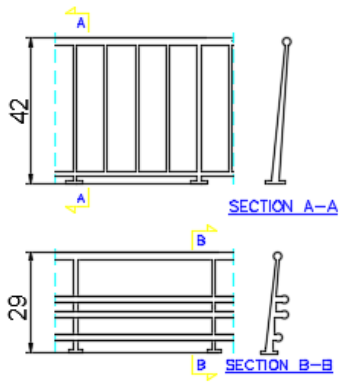

Figure 4. Railings used for the external decks (above) and the central deck (below). Dimensions are in mm

Force Coefficients

The drag, lift and moment force coefficients were measured in the forced motion rig under static conditions, i.e. no motion. The forces were measured along the body axis in 60 seconds at the following angles of attack: $\alpha = \{-6°, -5°, \ldots, 6°\}$ where α is the rotation of the bridge deck (positive nose up). The measured body forces were transformed to lift and drag, positive up and along the wind, respectively. The moments were measured and defined positive nose up. The force coefficients are given by

$$C_d = \frac{F_d}{qB}\ ;\ C_l = \frac{F_l}{qB}\ ;\ C_m = \frac{M}{qB^2} \qquad (1)$$

where $q = \frac{1}{2}\rho U^2$ is the incoming dynamic pressure, ρ is the density of air and U is the mean incoming wind speed. The mean values of the measured drag, lift and moment forces per unit length are denoted F_d, F_l and M respectively.

It was observed that the force coefficients were sensitive to the Reynolds number, $Re = UD_c/\nu$, where the characteristic length is the depth of the central box, $D_c = 0.04$m and $\nu = 1.5111 \cdot 10^{-5}$ m^2/s is the kinematic viscosity of air. The force coefficients dependency on the Reynolds number are shown in Figure 5 for $\alpha = 0°$ deg. At $\alpha < -3°$ deg angles of attack the section started shaking at $U \geq 15$ m/s which challenged a good estimation of the static force coefficients. Therefore, the only force coefficients shown in Figure 6 are the static force coefficients at $3200 \leq Re \leq 42000$. It is seen that the lift forces are linear, but the moment and drag forces are non-linear with respect to the angle of attack, α.

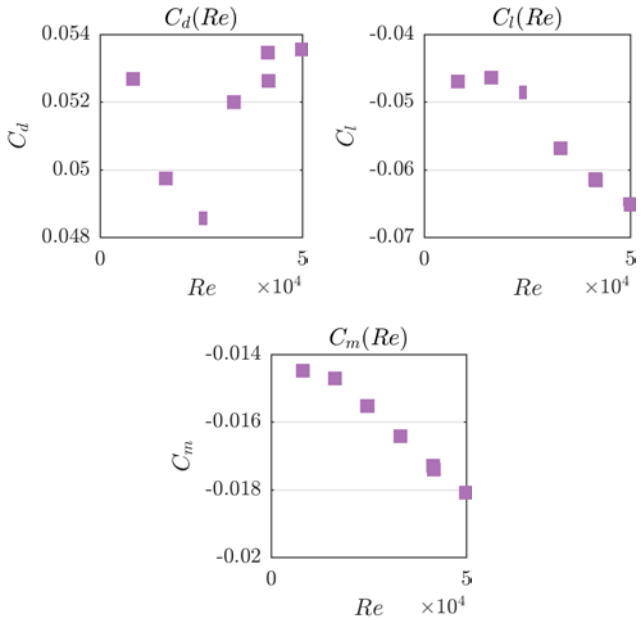

Figure 5. The scatter represents the lift coefficients obtained from the mean of the measured lift forces per unit length at zero degrees angle of attack ($\alpha = 0°$ deg) for different Reynolds numbers

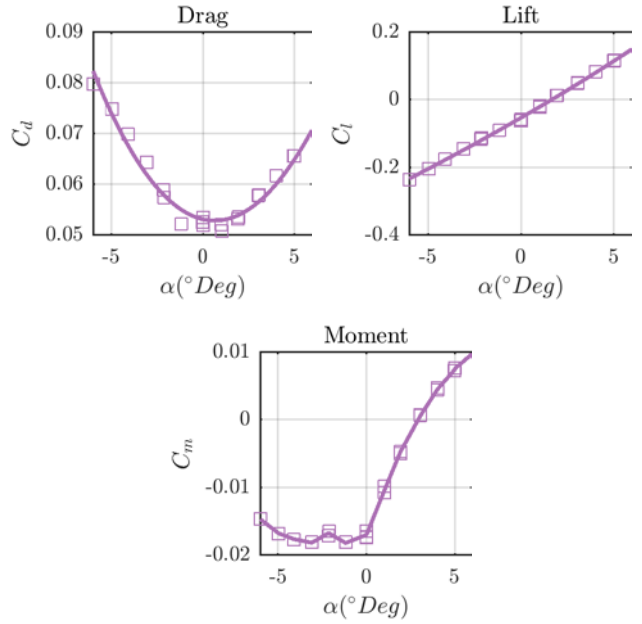

Figure 6. Static drag, lift and moment coefficients for the section model tested. Reynolds numbers effects might have caused small differences in the estimated coefficients indicated by the scattered values at the same angle of attack, α

Aerodynamic Derivatives

The full set of 18 aerodynamic derivatives at the mean angle of attack $\alpha = 0°$ deg. was estimated for the section using the 3D forced motion rig available in the wind tunnel. Prescribed single degree of freedom harmonic motion was used to excite the section model at different incoming wind speeds ranging from still air to $U \approx 15$ m/s. The lift, drag and moment force time histories were measured synchronously with the input motion. The transfer function, **E,** between the input motion, **X** and the output motion induced forces, **Y**, can be estimated in the time domain either by the least squares method [7] or simply by multiplying the output forces with the pseudo inverse of the input motion

$$\mathbf{E} = \mathbf{Y}\mathbf{X}^{+} \qquad (2)$$

where **X** is a 6×N matrix containing the velocity and displacement time histories in rows and **Y** is a N×3 matrix with the output force time histories and N is the number of samples in the discretised time histories. The sampling rate was $f_s = 200$ and the number of samples was $N = 12000$ for all measurements. If the noise in the measurement system is considered to be zero mean it averages out in the system identification. The inertia forces are estimated by still air tests and are subtracted from **E**. Finally, the aerodynamic derivatives are estimated from **E** following the same definitions as in [7].

With the pitching motion amplitude $\alpha = 2°$ deg., saw tooths were observed in the measured moment when $\alpha(t) < 0$ which is shown in Figure 7. This agrees well with the non-linear steady aerodynamic moment, $M(\alpha)$, in Figure 6 and gives rise to motion induced forces at other frequencies than at the harmonic motion frequency.

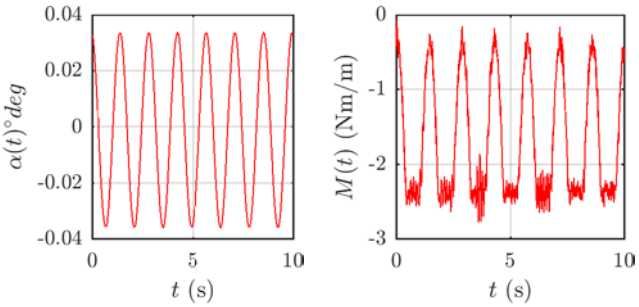

Figure 7. Time histories for the pitching motion (left) and measured moment (right) at $U = 14.58$ m/s

In order to get the transfer functions, **E**, between the motion and the motion induced forces at the motion frequency only, a digital linear phase fourth order bandpass filter was applied to the measured motion and forces prior to estimation of the transfer functions, **E**, and the aerodynamic derivatives. Rectangular windowing has been applied after filtering. The motion frequency was $f = 0.7\ Hz$ and the amplitudes of motion were 16mm for the vertical and lateral degrees of freedom. The filter employed allowed only frequencies between 0.4 Hz and 1.2 Hz to pass.

The aerodynamic derivatives, A_2^*, A_3^*, H_1^*, and H_3^*, which are considered to be the most important for torsional and classical flutter are shown in Figure 8.

The tendencies of the derivatives follow the flat plate with positive vertical and torsional damping and negative torsional aerodynamic stiffness. This is however only valid when the mean angle of attack is zero. The section is aerodynamically non-linear and the derivatives are susceptible to changes as the wind speed increases and pressures the section to rotate to mean values of $\alpha < 0°$deg. (nose down).

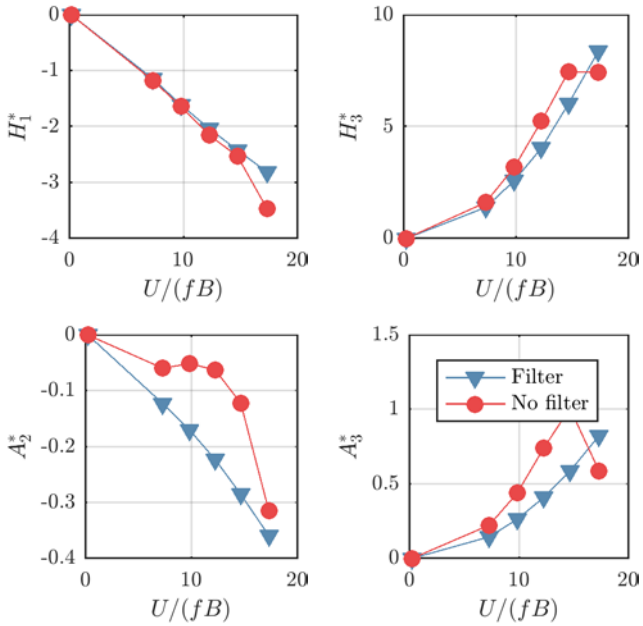

Figure 8. Aerodynamic derivatives estimated after digital linear phase bandpass filtering (triangles) and without digital filtering (circles)

Free Vibration Tests

The forced motion tests indicated that at $\alpha = 0°$ classical flutter may occur due to the sign of A_2^* and A_3^*. The static tests showed that non-linear steady and quasi-steady effects on the aerodynamic moment are expected when $\alpha < 0°$deg. The actual results from the free vibration tests may therefore differ considerable from the typical flat plate case with linear aerodynamic force coefficients.

The spring ratios and the equivalent mass and mass moment of inertia were estimated by free decay tests at different dummy mass configurations in still air.

The mechanical properties of the section model configured to four different torsional-to-vertical frequency ratios are presented in Table 1.

The highest reached reduced wind speeds in the tests are given by $\frac{U_{max}}{(f_h B)}$ in Table 1 where the still air natural vertical frequency is denoted f_h and $B = 1.2$m is the full width of the section.

Configuration	γ_ω	f_h	m_e	I_e	$\frac{U_{max}}{f_h B}$
A	0.97	1.35	7.57	1.27	12.54
B	1.10	0.89	7.63	1.29	17.17
C	1.21	0.89	7.63	1.29	17.82
D	1.55	1.55	4.64	0.45	13.40

Table 1. Mechanical properties of the section model in configuration A, B, C and D

The section model was suspended in springs connected to load cells which were calibrated to return the displacements for configuration A. Softer springs were installed to test configuration B, C and D at higher reduced wind speeds to simulate higher equivalent full scale wind speeds. In this case, the displacements given by the measurement system were calibrated to configuration A but since the displacements are proportional to the stiffness of the springs which are known, the displacements were corrected afterwards in the data processing. The section model was damaged by manual excitation during free decay testing at very high tunnel wind speeds. A repair was made

by gluing an aluminium plate (496 mm x 246 mm x 0.5 mm) to the bottom of the central box which slightly modified the shape of the cross section by adding 0.5 mm to the depth along 20% of the total length of the section model. The incident occurred between testing configuration A and B. The repair are considered to have negligible influence on the results.

In [1] we assumed that torsional or static divergence would occur instead of flutter when $\gamma_\omega < 1$ and that the critical wind speed for divergence could be postponed if the slope of the moment curve was reduced. Similarly we expected that classical flutter would occur when γ_ω were only slightly larger than 1. These assumptions were based on linear aerodynamics.

Neither divergence nor flutter was observed for the configurations in the present study. As the tunnel wind speed increased, the sections rotated with the nose down and entered the aerodynamic non-linear area where the slope of the moment coefficient decreases and eventually becomes negative as shown in Figure 6.

Configuration A responds faster to the steady aerodynamic moment due to the lower torsional stiffness. Since the slope of C_m values goes from positive to negative at $\alpha < -1°$ deg., limit cycle oscillations occurs until the mean rotations decreases further where it enters a stable regime with large mean displacements. Configuration B and C followed the same pattern, but without any limit cycle oscillations which most likely is due to the higher torsional stiffness. The highest tunnel wind speed for configuration C corresponds to an equivalent full-scale wind speed of approximately $U = 88$ m/s if the first bending frequency of the full-scale bridge deck structure is $f_b = 0.082$ Hz. The mean values and the standard deviations of the response for the different configurations are shown in Figure 9 against the reduced wind speed, $U_r = U/(f_h B)$.

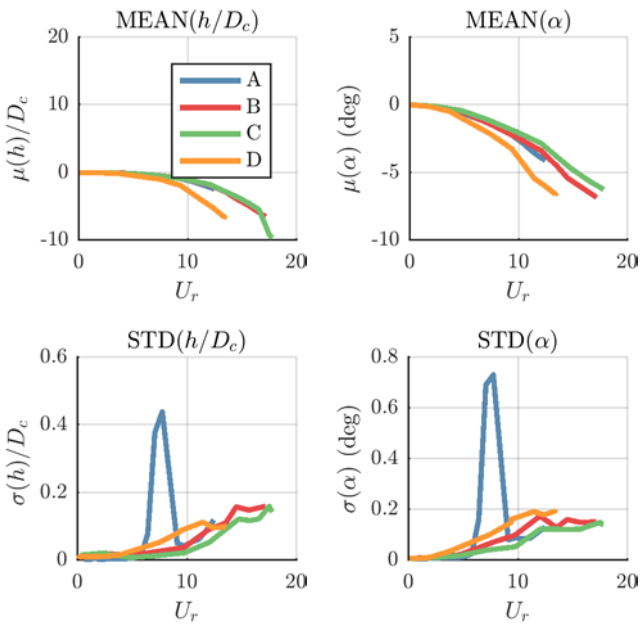

Figure 9. The mean vertical response relative to the depth of the central box girder, $\mu(h)/D_c$, are shown in the upper left plot. The mean rotations, $\mu(\alpha)$, are shown in the upper right plots. The lower plots shows the standard deviation of the vertical and torsional response. The legends in the upper left plot applies to all plots

The peak in the standard deviations for configuration A in Figure 9 indicates the limit cycle oscillations.

Conclusions

It is not possible to make the torsional frequency equal to the vertical or lower, without artificially reducing the torsional stiffness. This will cause the section to rotate at lower wind speeds compared to configurations with higher torsional stiffness. The non-flutter design principle where $\gamma_\omega \leq 1$ will avoid classical flutter and divergence might be avoided if the moment slope is flat, negative or non-linear, but the lack of torsional stiffness caused violent limit cycle oscillations for the present section.

The section model performed aerodynamically stable at a torsional-to-vertical frequency ratio, $\gamma_\omega = 1.21$, which is easily reached and exceeded for suspended spans between 2 and 4 km. Even in the extreme lightweight configuration D, the section performed stable at all wind speeds. Flutter is not a problem for this section. The best solution is therefore to enhance the torsional stiffness and the torsional-to-vertical frequency ratio to a level giving a satisfying static mean response. Future studies should investigate the Vortex Induced Vibrations of the section.

Acknowledgments

FORCE Technology and the employees, involved in the present project, are gratefully acknowledged for their kind and helpful support. We are thankful to COWIfonden for financial support and to Dr. Allan Larsen for valuable insight and guidance throughout the project.

References

[1] Andersen, M.S., Johansson, J., Brandt, A. & Hansen, S.O. Aerodynamic stability of long span suspension bridges with low torsional natural frequencies, *Engineering Structures.*, **120**, 2016, 82-91.

[2] Andersen, M.S., Sahin, E., Lenius, M. and Læsø, J.R. *Implementation of the non-flutter design principle*, IN-VENTO 2014, XIII Conference of the Italian Association for Wind Engineering, Genova, Italy, 2014.

[3] Bartoli, G., D'Asdia, P., Febo, S., Mannini, C., Pastò, S. & Procino, L. *Innovative solutions for long-span suspension bridges*, BBAA VI International Colloquium on Bluff Bodies Aerodynamics & Applications, Milano, Italy, 2008.

[4] Johansson, J., Andersen, M.S. & Øvre, M.S. *Non-flutter design principle for long span bridges*, APCWE8, Chennai, India, 2013.

[5] Larsen, A. & Larose, G. Dynamic wind effects on suspension and cable-stayed bridges, *Journal of Sound and Vibration*, **334,** 2015, 2-28.

[6] Richardson, J. R. *The development of the concept of the twin suspension bridge*. NMI R125, 1981.

[7] Siedziako, B., Øiseth, O & Rønnquist, A. An enhanced forced vibration rig for wind tunnel testing of bridge deck section models in arbitrary motion. *Journal of Wind Engineering and Industrial Aerodynamics*, **468**, 2017, 164-152.

[8] Walshe, D.E. & Wyatt, T.A. Bridge aerodynamics 50 years after Tacoma Narrows – Part II: A new discipline world-wide, *Journal of Wind Engineering and Industrial Aerodynamics*, **40**, 1992, 327-336.